1 Introduction

In computer vision and geometry processing, the representation of geometric shapes for various applications poses challenges, especially when dealing with tasks like shape comparison, symmetry detection, and shape classification. Common representations like meshes or point sets, while useful for visualization and rendering, fall short in these contexts because they do not inherently accommodate transformations such as rigid or isometric shifts. The paper proposes a novel Heat Kernel Signature (HKS) designed to capture the intrinsic geometry of a shape efficiently and multi-scale, focusing on the diffusion of heat over time to provide a natural scale of observation from local to broader neighborhood characteristics. This signature is stable under shape perturbations, concise yet informative, and invariant under isometric deformations, making it highly suitable for tasks involving deformable shapes. HKS leverages the heat kernel properties through temporal restrictions, enabling robust applications in shape registration, partial matching, and the detection of intrinsic symmetries across different shapes, providing a more reliable and computationally efficient approach than other local point signatures like Spin Images or Shape Context.

In our experiments, we analyzed two distinct meshes representing a cow mesh from coursework 2 and a human mesh [1]. The distribution of heat across these meshes is visualized using a color map, corresponding to different temperature ranges. This visualization is shown in Figure 1.

Figure 1: Color Map

2 Heat Operator and Heat Kernel

The analysis of heat diffusion on Riemannian manifolds requires a clear definition of the heat operator. This operator is characterized by the heat equation, expressed as:

$$\Delta_M u(x,t) = -\frac{\partial u(x,t)}{\partial t}$$

where Δ_M denotes the Laplace-Beltrami operator acting on the function $u(x,t)$, which represents the heat distribution at vertex x and time t. For boundary conditions, $\partial_M u(x,t) = 0$ is used to satisfy the Dirichlet conditions.

The heat operator H_t, applied to a function f, is given by:

$$H_t f(x) = \int_M k_t(x,y) f(y)\, dy$$

Here, $H_t f(x)$ can be interpreted as the heat distribution $u(x,t)$ at time t. The heat kernel $k_t(x,y)$, essential to this process, shows the diffusion characteristics over time and is defined through the eigenvalues λ_i and eigenfunctions $\phi_i(x)$ of the Laplace-Beltrami operator, as follows:

$$k_t(x,y) = \sum_{i=0}^{\infty} e^{-\lambda_i t} \phi_i(x) \phi_i(y)$$

Figure 2 illustrates the application of the heat operator, utilized for computing the heat at each vertex on the mesh at time t. Furthermore, Figure 3 presents a graph of the heat values at different vertices plotted against $\log(t)$, providing evidence that each vertex exhibits a distinct temporal heat distribution. These differing tendencies across vertices support the viability of using the heat operator for shape retrieval tasks.

Figure 2: Heat distribution with heat operator for cow and human meshes

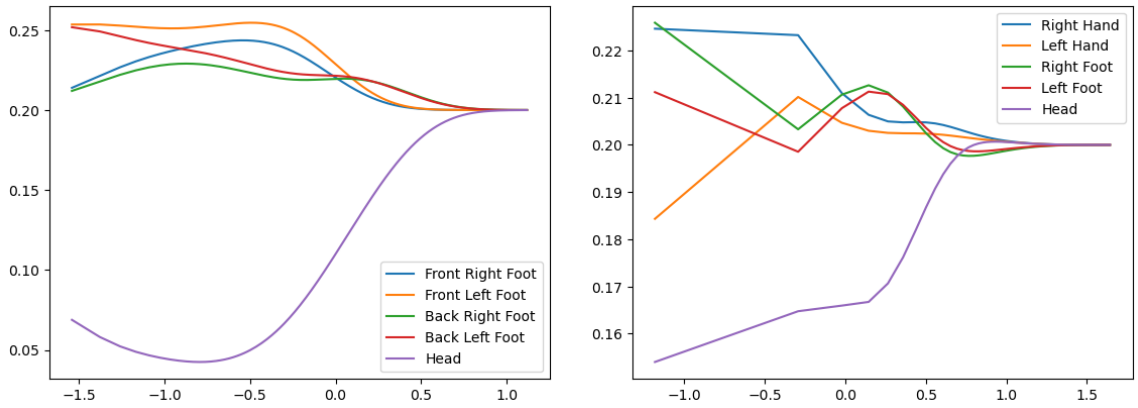

Figure 3: Change of heat with heat operator both on logarithmic for time

3 Heat Kernel Signature (HKS)

While the heat kernel $k_t(x, y)$ offers numerous advantages for analyzing the properties of a manifold, its complexity poses challenges for practical computations and comparisons. Specifically, $k_t(x, y)$ is a function on the Cartesian product of the temporal and spatial domains, $\mathbb{R}^+ \times M$, which results in a high-dimensional space that can be difficult to work with directly.

To address this issue, the paper [2] proposes a method to reduce this complexity by introducing the concept of the Heat Kernel Signature (HKS). The HKS is a function defined solely over the temporal domain for a fixed point x, significantly simplifying the comparison between signatures of different points. The HKS for a point x on the manifold is defined as follows:

$$HKS(x)\colon \mathbb{R}^+ \to \mathbb{R}, \quad HKS(x, t) = k_t(x, x)$$

Figure 4 demonstrates that, although the same time value of heat at various points shows slight differences, there is a notable similarity. Figure 5 further illustrates this by depicting the temporal flow of heat distribution under the heat kernel and the Heat Kernel Signature (HKS) using the mesh Laplace operator, which will be further explained in the next section. Both the heat operator and the HKS yield comparable results, even though the speed of heat flow slightly differs. Therefore, we can conclude that the HKS effectively reduces computation time while maintaining the performance of the traditional heat operator.

Figure 4: Comparison of heat value at time = 3 $k_t(x, y)$ (Left) and $HKS(x)$ (Right)

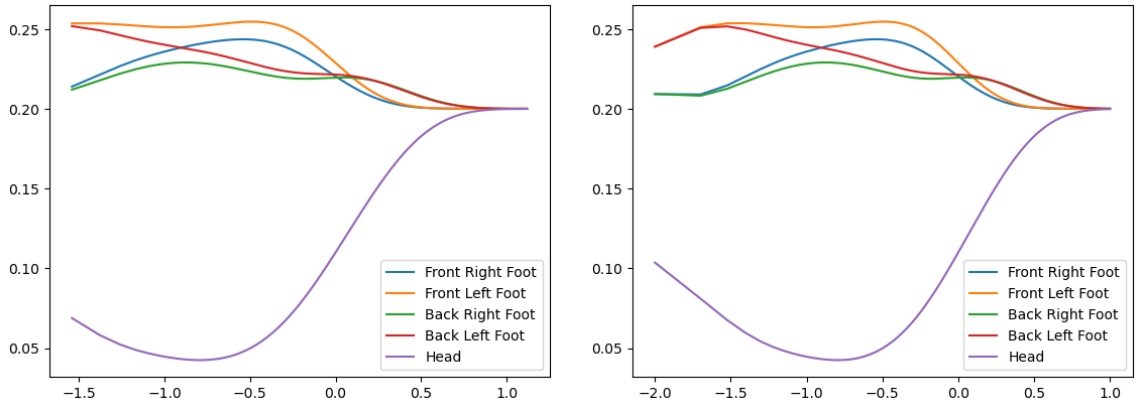

Figure 5: Plot of heat diffusion $k_t(x, y)$ (Left) and $HKS(x)$ (Right), both on logarithmic for time

4 Discrete Heat Kernel and Laplace-Beltrami Estimation

In computational geometry, the estimation of the Laplace-Beltrami operator is essential for manifold analysis. The cotangent scheme has been widely used due to its simplicity and ease of implementation, as referenced in coursework 2 and outlined by [3]. However, its convergence is depend on the quality of the mesh triangulation. To address this limitation, [4] proposed the mesh Laplace operator as a more robust alternative. The operator is defined in the discrete setting and offers an improved approximation of the continuous operator on a manifold.

The discrete heat kernel in a d-dimensional Euclidean space, denoted by $k_t(x, y)$, can be expressed as a Gaussian function. For a general compact manifold, the explicit form of the heat kernel may not be available, but it can be estimated using the mesh Laplace operator. This operator is

constructed as follows:

$$L = A^{-1}W$$

where A is a diagonal matrix with area weights, and W is the weight matrix derived from the mesh. The generalized eigenproblem associated with this operator yields a full set of eigenvectors and eigenvalues, which can be exploited to compute the heat diffusion process on the mesh.

The discrete approximation of the heat kernel is thus given by [4]:

$$L_K^h f(w) = \frac{1}{4\pi h^2} \sum_{t \in K} \frac{\text{Area}(t)}{\#t} \sum_{p \in V(t)} e^{\frac{-\|p-w\|^2}{4h}} (f(p) - f(w))$$

5 Multi-Scale Matching

In the context of multi-scale shape matching, it is important to compare vertices at different scales effectively. This paper introduces two heuristics for scaling the heat kernel $k_t(x, x)$, defined as $k_t(x, x) = \sum_{i=0}^{\infty} e^{-\lambda_i t} \phi_i^2(x)$. The first heuristic faces the challenge that the difference $|k_t(x', x') - k_t(x, x)|$ reduces exponentially with the increase of t. This reduction may result in the differences at larger scales being overshadowed by the more pronounced differences at smaller scales. To overcome this, the paper suggests scaling $k_t(x, x)$ by its integral over the manifold M, $\int_M k_t(x, x)\, dx$, thus normalizing it across all scales M to make a uniform contribution to the shape signature, also known as the heat trace at tizme t.

The second heuristic observes that at a fixed point x, the variation of $k_t(x, x)$ is considerable at small t values but decreases as t increases. This occurs because $k_t(x, x)$ reflects the average heat value within a neighborhood whose size is determined by t. Given that average behavior in smaller neighborhoods is more susceptible to changes, the paper advocates for a logarithmic scaling of the temporal domain. This scaling yields a more consistent representation of the heat kernel signature (HKS), particularly when the signature exhibits more rapid changes at smaller scales.

$$d_{[t_1,t_2]}(x, x') = \left(\int_{t_1}^{t_2} \left(\frac{|k_t(x, x) - k_t(x', x')|}{\int_M k_t(x, x)\, dx} \right)^2 d \log t \right)^{1/2} \tag{1}$$

6 Evaluation

6.1 Evaluation on Gap of time interval for scaled difference

Figure 6 shows the difference in the Heat Kernel Signature (HKS) across the surface of a human mesh model, focusing on a vertex at the foot. These fluctuations are represented using equation 1, where the choice of the temporal gap between t_1 and t_2 is crucial. The resulting plot shows that when the temporal gap is too small, the heat variation is not distinct enough to differentiate between similar body parts such as the hand and foot. Conversely, with an optimally chosen gap, the HKS effectively highlights the differences between various mesh regions, which improves shape retrieval performance. However, if the gap is overly large, it becomes difficult to discern specific features on the mesh, thereby impeding accurate identification.

Similarly, Figure 7 shows that an optimally selected gap between t_1 and t_2 can yield a scaled heat value that accurately differentiates each part of a cow mesh at the vertices. Conversely, gaps that

are either too large or too small do not provide a clear distinction, thus affecting the effectiveness of the signature identification.

Figure 6: Scaled difference of HKS from foot, Left: Gap is small Center: Gap is middle Right: Gap is big

Figure 7: Scaled difference of HKS from front foot, Left: Gap is small Center: Gap is middle Right: Gap is big

Figure 8 shows the distribution of heat over time at various vertices, highlighting that corresponding points tend to achieve similar heat values as time progresses, ultimately converging to a uniform value across all points. Notably, the cow mesh's four vertices on each foot exhibit less variability in heat distribution compared to those on the human mesh. In particular, the vertices on the cow's feet show more consistent heat values than those on the human mesh's hands and feet.

Consequently, it is evident from Figures 6 and 7 that if the time interval between t_1 and t_2 is too narrow, the graph shows insufficient heat disparity to discern between individual vertices on the mesh. Conversely, if the interval is excessively wide, the scaled heat differences between various mesh regions become indistinguishable. This lack of distinction is attributable to the tendency of heat levels to stabilize over time; as shown in Figure 8, most vertices reach a similar heat value at extended timescales, leading to comparable integral results at t_1 and t_2.

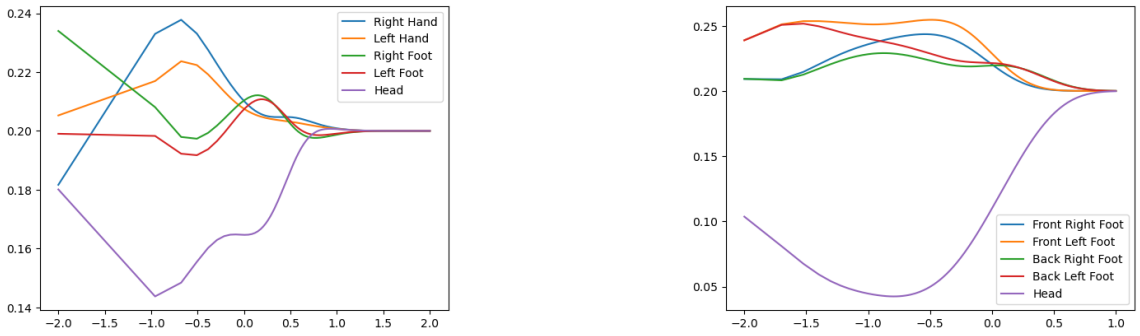

Figure 8: Change of heat as time pass, Left: Human, Right: Cow, both on logarithmic for time

6.2 Evaluation with MDS graph

In this section, we utilize Multi-Dimensional Scaling (MDS) from the `sklearn.manifold` library to analyze distinct vertex regions across three human meshes, each with a different pose. The MDS graph provides a evidence that illustrates the effectiveness of the Heat Kernel Signature (HKS) in identifying corresponding parts of each mesh, even when the mesh undergoes significant deformation. Figure 9 shows the meshes used for generating the MDS graph, highlighting the adaptability and precision of this analytical approach.

Figure 9: Different poses of human meshes [1]

Figure 10 demonstrates that, even when the meshes are deformed, the HKS calculated at the same time interval and at the same point on each mesh consistently locates in similar regions of the MDS graph. This consistency highlights the effectiveness of HKS in maintaining reliable identification across varying poses, underscoring its utility for shape analysis and deformation-invariant mesh comparison.

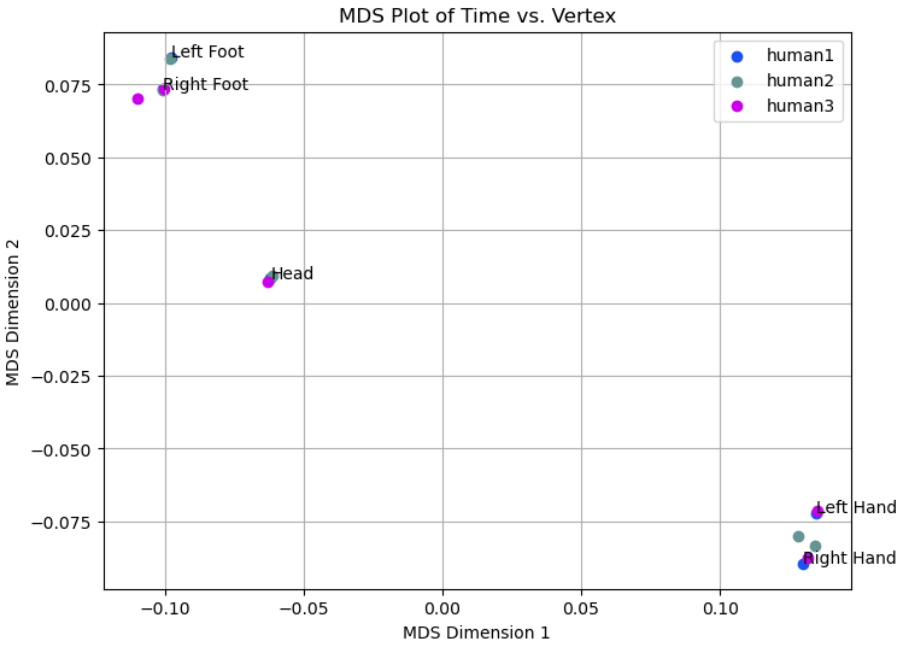

Figure 10: MDS graph for various vertices on different human meshes

7 Extension

7.1 Bag of Features

The Heat Kernel Signature (HKS) provides a means to reduce the computational cost associated with the heat operator, facilitating an effective method for the identification and retrieval of shape signatures. Direct application of HKS for mesh classification tasks is not straightforward; hence, we adopt the bag of features strategy, as introduced by [5], to extract mesh features informed by HKS.

To implement this, for each vertex x on the shape, HKS has to be computed as an n-dimensional descriptor vector $p(x) = (p_1(x), ..., p_n(x))^T$. The elements of this descriptor vector are given by

$$p_i(x) = c(x)K_{\alpha^{i-1}t_0}(x, x),$$

where $c(x)$ is a normalization constant ensuring that the 2-norm of $p(x)$ is equal to 1, i.e., $\|p(x)\|_2 = 1$. In our experiments, the parameters are set to $t_0 = 10$ and $\alpha = 1.32$.

Then perform k-means clustering on the $p(x)$, where the chosen value of K corresponds to the feature vector's dimensionality in the bag of features schema. To implement K-mean algorithm, we adopt KMeans from `sklearn.cluster`. From here we can obtain number of centroid from k-mean algorithm $P = \{p_1, ..., p_K\}$. The feature distribution for each point x with its descriptor $p(x)$ is defined as $\theta(x) = (\theta_1(x), ..., \theta_K(x))^T$. This is a $K \times 1$ vector, with its elements computed as

$$\theta_i(x) = c(x)e^{-\frac{\|p(x)-p_i\|^2}{2\sigma^2}},$$

where $c(x)$ is again a normalization constant, but this time it ensures that the 1-norm of $\theta(x)$ is equal to 1, $\|\theta(x)\|_1 = 1$. The parameter σ governs the "softness" of the assignment of descriptors to vocabulary elements.

Therefore, process of converting the entire shape X into a bag of features which is V $\times$ 1 vector can be expressed as function:

$$f(X) = \int_X \theta(x) da(x)$$

7.2 Evaluation

To evaluate the performance of the Heat Kernel Signature (HKS) combined with the bag of features approach, we utilized a dataset referenced in [6], which gives a variety of annotated mesh types. For simplicity and to limit processing time, we set $K = 10$. We employed a nearest neighbor algorithm by using KNeighborsClassifier `sklearn.neighbors` with 11 neighbors using the L1 loss function. The dataset is categorized into seven classes: Santa, horse, dog, bird, laptop, female, and male (Figure 11). Figure 12 displays the Precision-Recall (PR) curve for each class, plotted using the top K method.

Figure 11: Dataset classes for Mesh Classification

According to the results shown in the PR curves, the model generally delivers reasonable performance; however, it cannot be considered as exhibiting outstanding performance. This suboptimal performance can be attributed to three main factors. Firstly, the small size of our training set, consisting of only 72 datasets, may have adversely impacted the performance since the KNN algorithm is known to be sensitive to the size of the training dataset. Also, we use 10 for K-mean which can be lack of centroid to represent the meshes. Additionally, the presence of varying scales within the same class of meshes may have further compromised the effectiveness of the HKS, as indicated in [7].

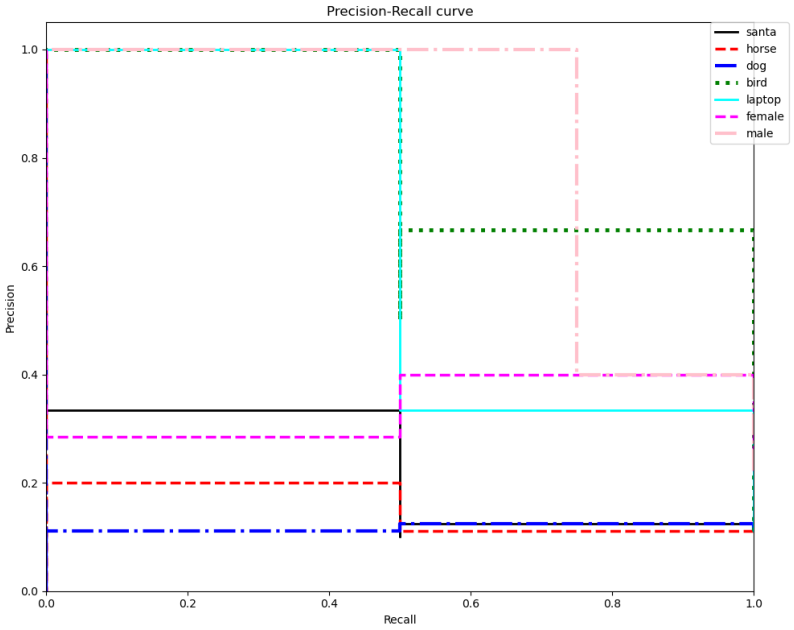

Figure 12: PR curve for each classes

8 Conclusion

We successfully implemented the method described in "A Concise and Provably Informative Multi-Scale Signature Based on Heat Diffusion" [2]. The Heat Kernel Signature (HKS) offers a similarly accurate yet computationally less expensive method for calculating heat over time. However, applying HKS directly to mesh classification tasks presents challenges due to its limitations; consequently, we incorporated the bag of features approach [5] and effectively assessed the performance of HKS on mesh classification tasks.

Despite its advantages, HKS has several limitations, including its lack of scale invariance and the inability to compute heat for meshes when eigenanalysis is not feasible. Nonetheless, HKS provides significant motivation for advancing shape retrieval tasks.

References

[1] D. Vlasic, I. Baran, W. Matusik, and J. Popović, "Articulated mesh animation from multi-view silhouettes," *ACM Trans. Graph.*, vol. 27, no. 3, p. 1–9, aug 2008. [Online]. Available: https://doi.org/10.1145/1360612.1360696

[2] J. Sun, M. Ovsjanikov, and L. Guibas, "A Concise and Provably Informative Multi-Scale Signature Based on Heat Diffusion," *Computer Graphics Forum*, 2009.

[3] G. Xu, "Discrete laplace–beltrami operators and their convergence," *Computer Aided Geometric Design*, vol. 21, no. 8, pp. 767–784, 2004, geometric Modeling and Processing 2004. [Online]. Available: https://www.sciencedirect.com/science/article/pii/S0167839604000810

[4] M. Belkin, J. Sun, and Y. Wang, "Discrete laplace operator on meshed surfaces," in *Proceedings of the Twenty-Fourth Annual Symposium on Computational Geometry*, ser. SCG '08. New York, NY, USA: Association for Computing Machinery, 2008, p. 278–287. [Online]. Available: https://doi.org/10.1145/1377676.1377725

[5] M. Ovsjanikov, A. Bronstein, M. Bronstein, and L. Guibas, "Shape google: A computer vision approach to isometry invariant shape retrieval," 11 2009, pp. 320 – 327.

[6] D. Pickup, X. Sun, P. Rosin, R. Martin, Z. Cheng, S. Nie, and L. Jin, "Shrec'15 track: Canonical forms for non-rigid 3d shape retrieval," 05 2015.

[7] M. Bronstein and I. Kokkinos, "Scale-invariant heat kernel signatures for non-rigid shape recognition," 06 2010, pp. 1704–1711.